

Original Article

A system for evaluating magnetic resonance imaging of prostate cancer using patient-specific 3D printed molds

Alan Priester¹, Shyam Natarajan², Jesse D Le², James Garritano¹, Bryan Radosavcev³, Warren Grundfest¹, Daniel JA Margolis⁴, Leonard S Marks², Jiaoti Huang³

¹Department of Bioengineering, University of California Los Angeles, CA, USA; Departments of ²Urology, ³Pathology, ⁴Radiology, David Geffen School of Medicine, Los Angeles, USA

Received June 4, 2014; Accepted June 25, 2014; Epub July 12, 2014; Published July 15, 2014

Abstract: We have developed a system for evaluating magnetic resonance imaging of prostate cancer, using patient-specific 3D printed molds to facilitate MR-histology correlation. Prior to radical prostatectomy a patient receives a multiparametric MRI, which an expert genitourinary radiologist uses to identify and contour regions suspicious for disease. The same MR series is used to generate a prostate contour, which is the basis for design of a patient-specific mold. The 3D printed mold contains a series of evenly spaced parallel slits, each of which corresponds to a known MRI slice. After surgery, the patient's specimen is enclosed within the mold, and all whole-mount levels are obtained simultaneously through use of a multi-bladed slicing device. The levels are then formalin fixed, processed, and delivered to an expert pathologist, who identifies and grades all lesions within the slides. Finally, the lesion contours are loaded into custom software, which elastically warps them to fit the MR prostate contour. The suspicious regions on MR can then be directly compared to lesions on histology. Furthermore, the false-negative and false-positive regions on MR can be retrospectively examined, with the ultimate goal of developing methods for improving the predictive accuracy of MRI. This work presents the details of our analysis method, following a patient from diagnosis through the MR-histology correlation process. For this patient MRI successfully predicted the presence of cancer, but true lesion volume and extent were underestimated. Most cancer-positive regions missed on MR were observed to have patterns of low T2 signal, suggesting that there is potential to improve sensitivity.

Keywords: MRI, prostate cancer, whole mount, registration, pathology, 3D printing

Introduction

Historically, prostate cancer (CaP) has been diagnosed with a series of needle biopsy cores placed under ultrasound guidance [1]. However, in recent years the diagnosis and treatment of CaP has been transformed by the advent of advanced imaging techniques and precise targeting devices.

Increasingly, medical imaging data is being utilized in the decision pathway as a diagnostic aid [2-5], pre-surgical staging tool [2, 6], or to evaluate cancer recurrence [7, 8]. It has been demonstrated that multiparametric MRI (mpMRI) is a highly sensitive means of prospectively identifying areas of cancer within the prostate [3, 9, 10]. In order to better understand the underlying phenomena and to improve the imaging methods, correlation with

the true cancer extent is necessary. MRI-histopathology correlation, typically performed using whole mount sections of post-prostatectomy specimens, is either used to evaluate the accuracy of the imaging test, or to assess the imaging characteristics of known cancer.

Numerous techniques of MRI-histology correlation have been reported, either relying on sector-based analysis of lesion locations [9, 11], digital mapping of cancer coordinates from one modality to another (registration) [12-15], or improved tools for gross sectioning [16-18]. The first approach is limited by imprecise knowledge of the true cancer location, while the second requires knowledge of the cutting plane during gross sectioning. The third approach can help regulate the cutting plane, but does not account for morphological changes during the fixation process.

3D printed molds for MR-histology correlation

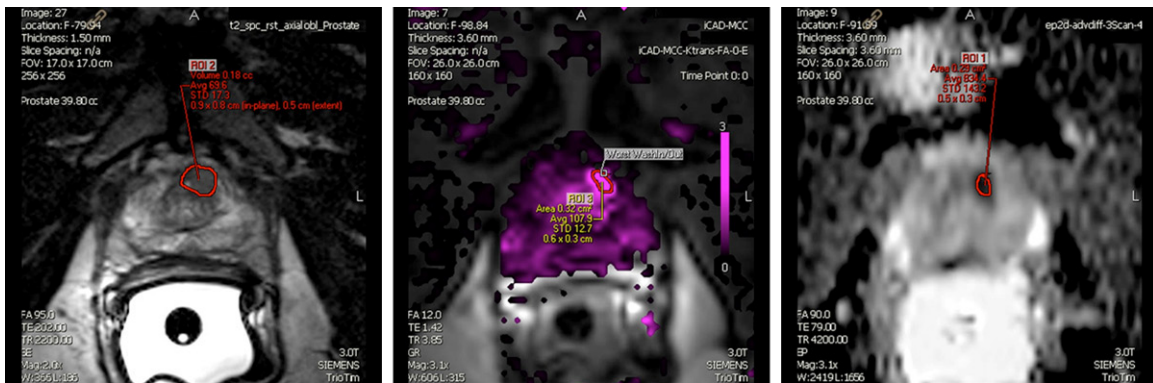


Figure 1. Region of suspicion on T2-weighted (left), K_{trans} (middle), and DWI (right) imaging.

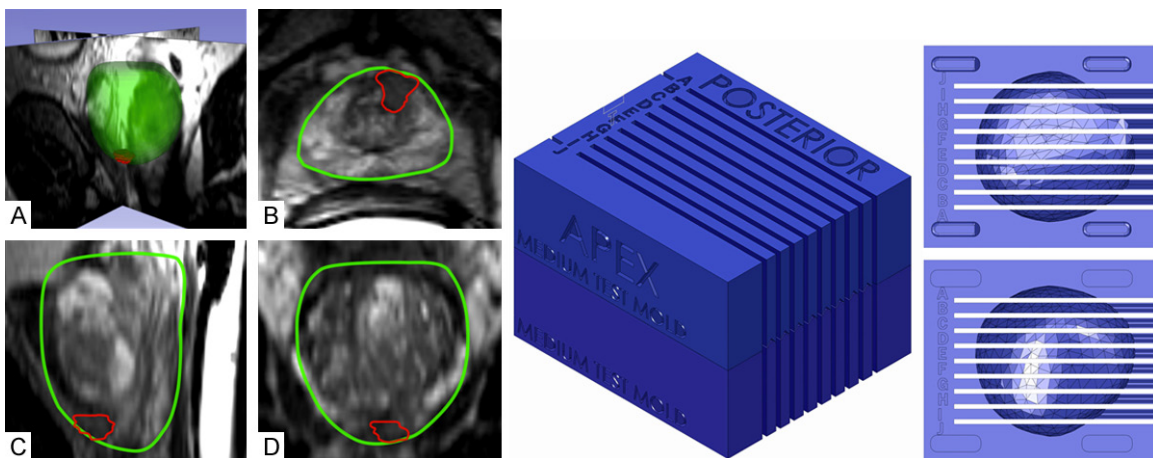


Figure 2. Left: The patient's 3D prostate surface (A) and the contours used to generate it in transverse (B), sagittal (C), and coronal (D) views. Right: A patient-specific 3D printed mold with parallel slits and a prostate cavity in the inner surface.

In order to address this problem, a group has reported on the use of patient-specific 3D-printed molds to improve gross sectioning and registration [18, 19]. However, a recent review on MRI-histology co-registration techniques describes potential sources of error, even when using both registration and sectioning aids [20]. Prior studies rely on expensive 3D printed molds, and do not account for shifting of the remaining prostate tissue as it is serially sectioned. Furthermore, this technique does not necessarily account for morphologic changes during specimen resection, grossing, and fixation. Herein, we describe the use of a low-cost patient-specific prostate mold, a hinged multi-bladed sectioning device, and an elastic registration technique for precise, quantitative MR-histology correlation.

Correlation methodology

The case of one patient, a 54-year old man, is reported here to illustrate our correlation methodology. Following 12-core systematic biopsy, the patient was diagnosed with Gleason 3+3 = 6 disease in a single positive core. Subsequently, the patient received a 3T multiparametric MRI with an endorectal coil (**Figure 1**), generating full field views of axial T1-weighted and T2-weighted images. Diffusion-weighted images (DWI) were also obtained, and pharmacokinetic maps with associated enhancement curves (K_{ep} , K_{trans}) were generated after administration of glucagon and gadopentetate dimeglumine (Magnevist, Bayer). A region in the left peripheral anterior gland was scored 4/5 on T2, DWI, and enhancement curves, using a

3D printed molds for MR-histology correlation

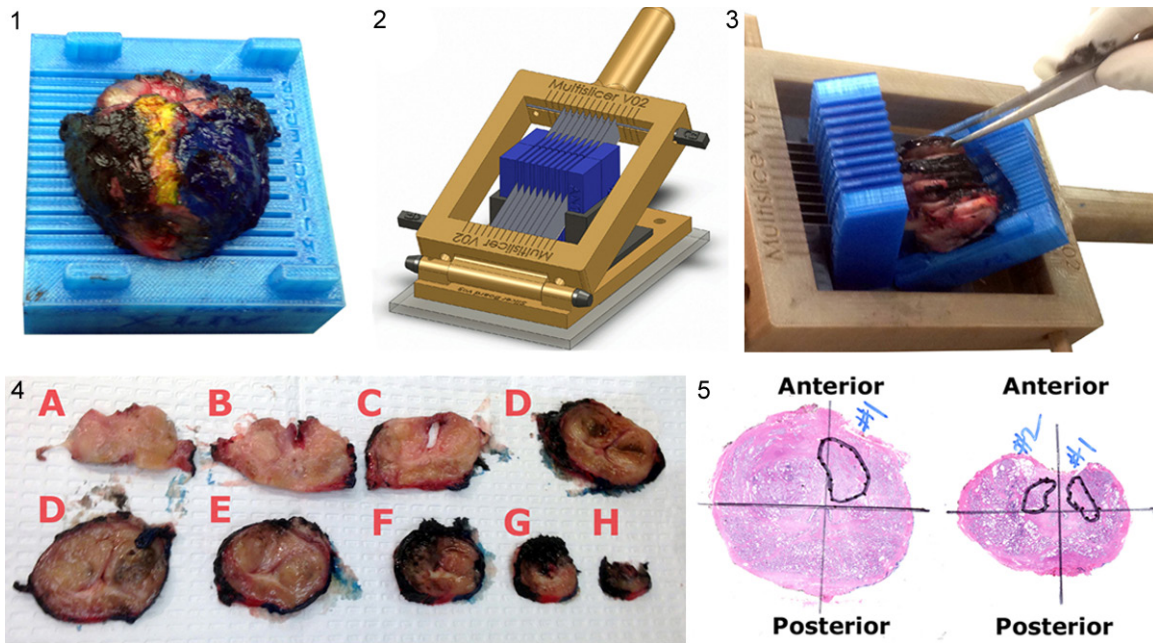


Figure 3. Illustration of the grossing process. An inked and trimmed prostate was placed within the patient-specific mold (1). Then the multi-bladed slicing device was used to acquire thin parallel whole-mount levels (2), which were removed from the mold (3) and labeled (4). These levels were then processed into slides, which were examined and annotated by an expert pathologist (5). The patient in this case had two apical slides showing cancer, with two distinct Gleason 3+3 = 6 lesions.

Likert-like scale previously described [21]. This indicated a high level of suspicion for cancer, and it was observed to be clinically organ-confined. The patient elected treatment and was scheduled to receive a radical robotic prostatectomy.

Design and manufacture of patient-specific prostate mold

First, the prostate boundary was manually delineated on the high-resolution T2-weighted image volume using commercial software (Profuse, Eigen, Grass Valley CA). The same image series was used to outline a single Region of Interest (ROI) in the anterior apex. Two 3D volumes were then generated from the prostate and ROI contours (**Figure 2**), and coordinates of the MR imaging planes relative to the surfaces were recorded.

The 3D prostate contours, i.e. segmentations, were imported into computer-aided design software (SolidWorks, Dassault Systèmes, Vélizy France). Within a rectangular mold, a cavity was then generated which matched the MR prostate surface exactly. This mold, seen in **Figure 2** and based on the work of Trivedi et al.

[19], was designed to hold the prostate in the same shape and orientation observed on MRI. It was manufactured in two halves, with the cavity roughly centered, to ensure easy placement and removal of specimen. The series of slits along its length, spaced 4.5 mm apart, correspond to predetermined MR imaging planes. The left, right, posterior, anterior, cranial, and caudal surfaces of the mold were clearly labeled to ensure correct specimen positioning.

The mold was manufactured from polylactic acid plastic using the Replicator 2, a consumer-grade 3D printer (Makerbot Industries, Brooklyn NY). The 3D printer extruded a 0.2 mm strand of molten plastic which rapidly cooled, building the two mold halves layer by layer. Printing was completed in advance of the surgery, and the mold was delivered to the grossing room.

Histological processing of prostate specimen

The specimen, freshly excised following radical prostatectomy, was delivered to the grossing room less than an hour post-surgery. Over the course of 10 minutes, a high-resolution 3D model of the prostate surface was then gener-

3D printed molds for MR-histology correlation

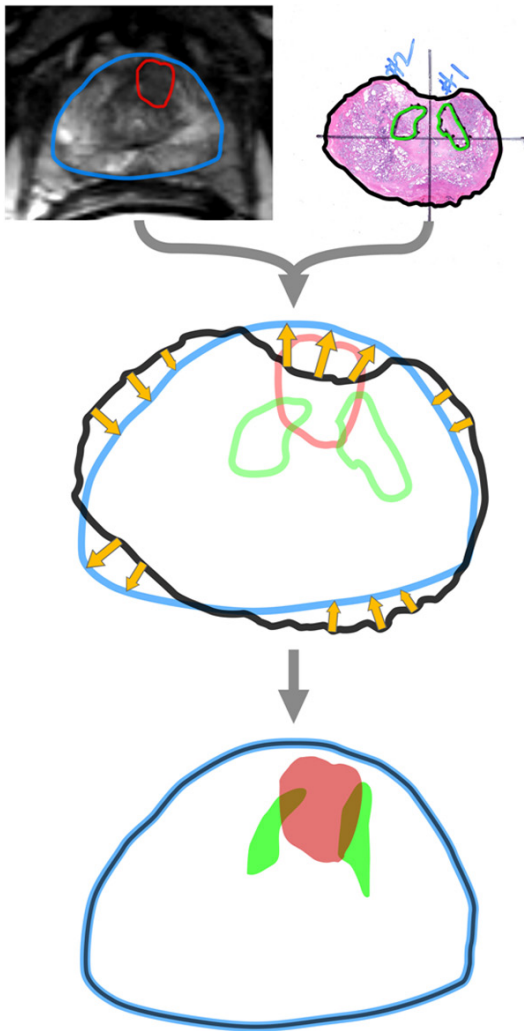


Figure 4. Illustration of elastic registration and the resulting warped contours. The MR prostate contour (top left) and the histology contour (top right) were superimposed using an affine transform based on centroids. The histological prostate surface was then warped (middle) to fit the MR contour, with arrows illustrating the effect of the warp. The bottom image shows the elastically warped histology targets, now in MR image space.

ated using a Digitizer 3D scanner (Makerbot Industries, Brooklyn NY). The specimen was then inked, blue on the left side and black on the right side, with red and yellow stripes on the midline posterior and anterior, respectively. The seminal vesicles were removed, and 2-3 mm of the apex were shaved to assess surgical margins. A second 3D scan was then performed to assess the effect of these initial grossing steps.

The specimen was placed within the mold such that the inked anatomy matched the external mold labels. The mold was then transferred to

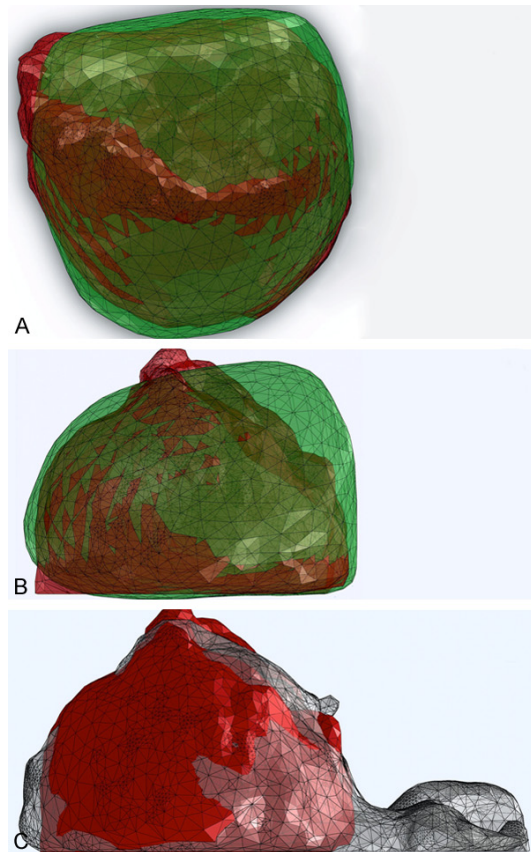


Figure 5. Coronal (A) and Sagittal (B & C) views of the MR prostate contour and 3D scan of the excised prostate surface. The MR prostate surface is seen in green. The excised prostate surface is seen in grey and red, before and after (respectively) removal of the seminal vesicles and shaving of the apex.

the cradle of a custom-designed, 3D printed, multi-bladed slicing device (**Figure 3**). The hinged device can accommodate up to 15 blades, allowing simultaneous acquisition of all slices. This confers a considerable advantage, as it prevents specimen displacement during slicing even in the presence of nodules. After operation of the slicing device, 10 evenly spaced, parallel levels were produced. Two of these were reserved for genetics research, and the remaining high-quality levels were formalin-fixed and paraffin embedded. Upon examination of the slides, an expert pathologist identified two lesions. Both were from apical levels, Gleason grade 3+3 = 6, and centered in the anterior prostate. Each slide was annotated with lesion contours and prostate orientation, then imaged with a flatbed scanner. **Figure 3** illustrates the grossing process and the resulting slides that were positive for cancer.

3D printed molds for MR-histology correlation

Table 1. 3D Scan Metrics

	MR Surface	Original Path	Processed Path
Volume (cc)	43.86	42.65	36.91
Apex to Base Axis (mm)	47.81	45.62	44.83
Anterior to Posterior Axis (mm)	33.87	33.16	35.55
Left to Right Lateral Axis (mm)	46.65	47.85	47.85
Optimum MR Overlap (%)	—	79.9%	77.3%

Metrics comparing the MR surface and prostate specimen (before and after apex shaving and removal of seminal vesicles).

MR-histology correlation

After manual segmentation of the prostate and lesion contours for each slide, MR-histology registration was automated using custom software, written using MATLAB 2013a (Mathworks, Natick MA). Several key assumptions were made:

1. Each slide was the apical surface of evenly spaced, parallel prostate levels.
2. All slides represented a complete prostate surface.
3. The prostate could shift at most one level's width (4.5 mm) within the mold, and this was corrected by aligning with the MRI to minimize surface area mismatch.
4. Variations in prostate shape relative to the MRI were due to tissue deformation during the grossing process, and were corrected with elastic warping algorithms.

Each image of the histological contours was loaded, projected onto the same plane as the corresponding MR slice, and then elastically registered in order to account for tissue deformation (**Figure 4**). The ROI identified on MR was then compared with the histological lesions using both surface and volume-based metrics. Lesion volumes were constructed by interpolating the space between known contours. All analyses were performed in the MR frame of reference, enabling retrospective scrutiny of false-positive and false-negative regions.

Results

The 3D scans, seen in **Figure 5**, demonstrated that the preoperative MR prostate segmenta-

tion was a good approximation of the excised specimen. The longest axes of the specimen matched those of the MR surface almost exactly (**Table 1**), indicating that the prostate would precisely fit the 3D printed mold. Volume on MR (43.9 cc) was seen to be larger than specimen volume (36.9 cc) after shaving of the seminal vesicles. However, a mean 10% reduction in volume due to surgical resection is to be expected [22]. Removal of the seminal vesicles was not observed to adversely affect the specimen's match to MR, and apex shaving was minimal (2.5 mm thickness).

After co-registration, it was evident that both lesions identified on histology were in close proximity to the ROI. **Figure 6** shows the interpolated series of ROI and lesion profiles, and **Figure 7** shows the 3D reconstructed lesion volume. A clear overlap between the ROI and lesion was observed on multiple levels, and the centroids of the interpolated volumes were only 5.6 mm apart. For most purposes this level of accuracy would be considered a targeting success, since the multiparametric MRI information correctly predicted the lesion's presence.

However, the MR images did not predict the presence of the disconnected satellite lesion, nor did lesion shape and extent match the ROI with good fidelity. Though the MR reading predicted a 0.5 mm out-of-plane extent, on histology the lesion appeared to span at least twice that distance; its true extent is unknown due to sparse depth sampling. Furthermore, the interpolated lesion volume (0.39 cc) on histology was nearly double the 0.21 cc predicted on MR. Despite their close proximity, only 6% of the histological lesion volume directly overlapped the ROI volume. However, levels that did contain lesions and ROI contours tended to have similar centroids, axis lengths, and areas, with a maximum overlap of 41% (**Figure 6**, level 13).

Discussion

MR-histology correlation is largely motivated by the desire to improve the predictive value of MRI. Refined visualization and interpretation of tumors on MRI could improve the utility of imaging, and potentially give rise to computer-aided detection tools. Furthermore, many studies

3D printed molds for MR-histology correlation

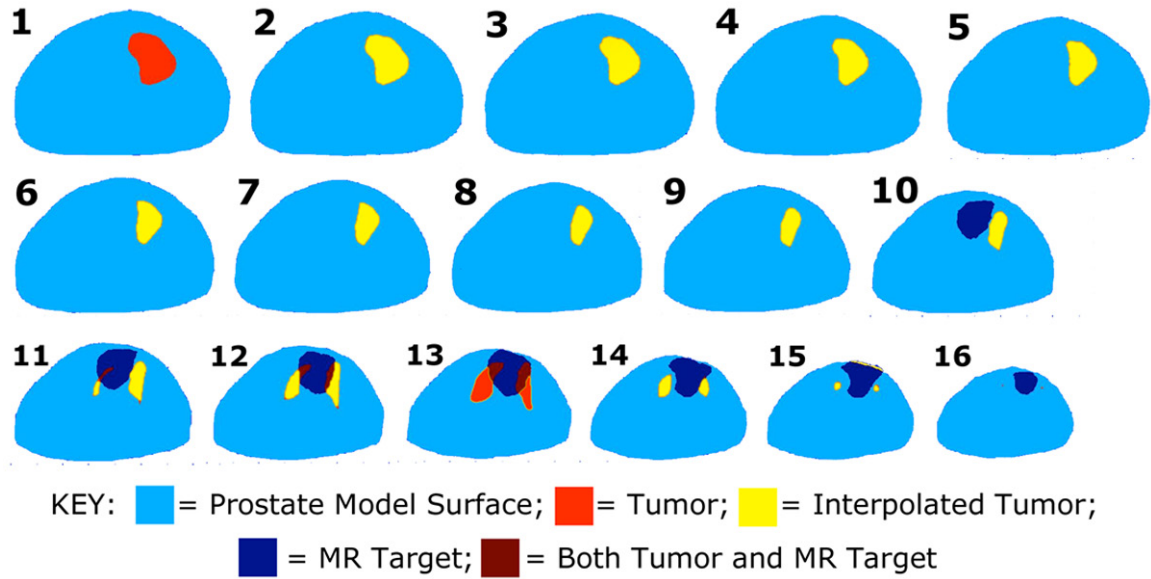


Figure 6. Lesion and ROI contours, progressing in 0.75 mm increments from midgland to apex.

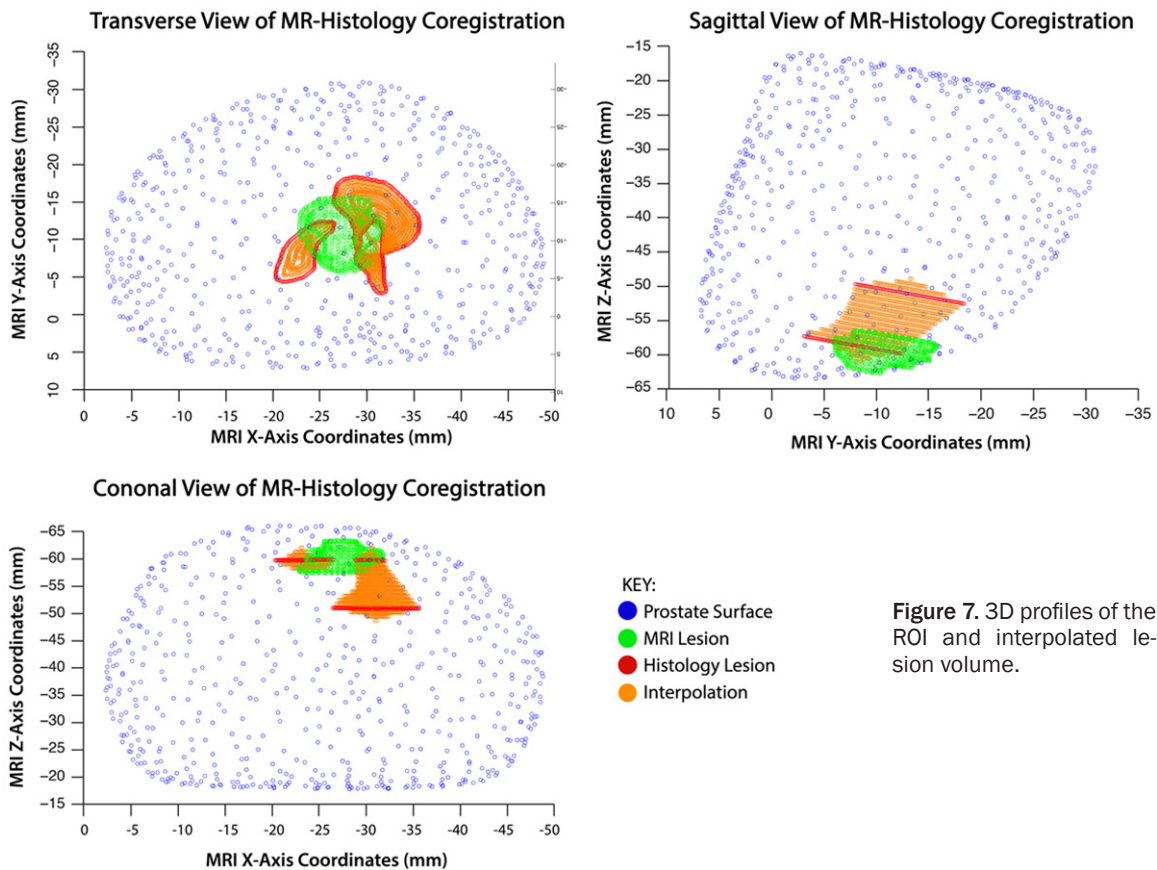


Figure 7. 3D profiles of the ROI and interpolated lesion volume.

note a marked false-negative rate of MRI for CaP diagnosis, with sensitivity ~50% for all lesions and ~75% for high-grade lesions [23,

24]. Accurate spatial correlation can help us understand the limitations of imaging, so that it may be used appropriately.

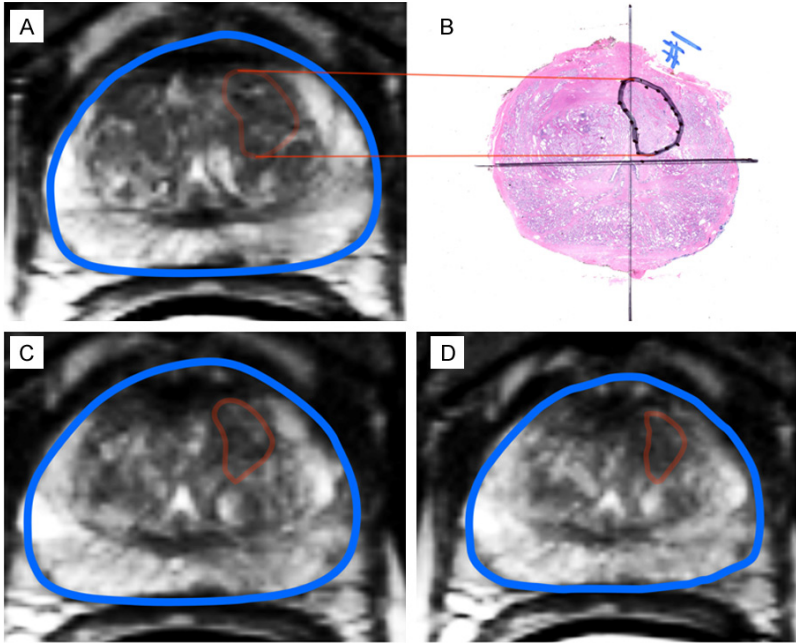


Figure 8. Low T2 signal levels in image areas proven to be cancer-positive (A and B) and in areas assumed to be positive using interpolation between known lesions (C and D).

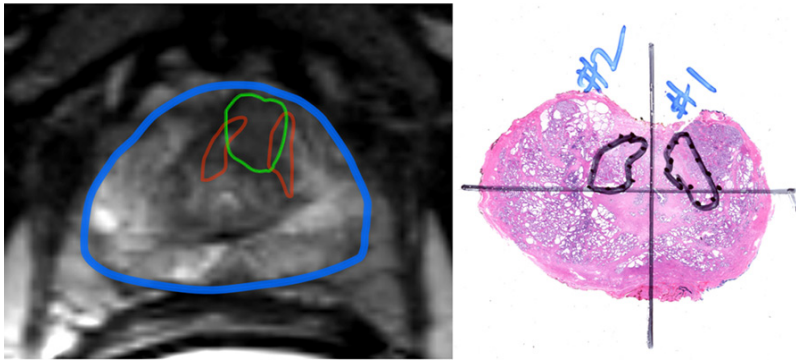


Figure 9. Illustration of the potential difficulty in distinguishing a true positive from a false positive region, with histology level (right) warped and co-registered to MR (left). Only the red regions were positive for cancer on histology, but no recognizable pattern was present to differentiate them from the green ROI on MRI.

To that end, each lesion contour was overlaid directly on the corresponding MR image, and examined for discernable patterns. As seen in **Figure 8**, the false-negative midgland levels had noticeably lower T2 intensity in areas positive for cancer. This suggests that if the region of suspicion had been segmented more aggressively, correlation accuracy could have been improved. However, as seen in **Figure 9**, in the apex it does not seem possible to distinguish false positive from true positive tissue. This suggests that, at least in this case, the sensitiv-

ity but not specificity could have been improved by careful analysis of the T2 image data.

It is important to note the limitations with the methodology presented here. Previous studies have noted that the *ex vivo* shape of the prostate is considerably different from the *in vivo* contour [22, 25]. This is exacerbated by use of an endorectal coil, which compresses the prostate [26]. To address this concern, Fan et al used a 9.4T *ex vivo* MRI to co-register the histopathology with *in vivo* MRI [27]. However, even with knowledge of *ex vivo* prostate geometry, the deformation of internal structures is still uncertain [13, 20]. Gibson et al improved this coregistration process by using artificial internal (gadolinium-soaked thread) and external (lamb kidney) fiducials [25, 28]. While reported to be accurate within a millimeter, this technique cannot be easily replicated at most institutions and disrupts normal pathology workflow.

Theoretically, using a patient-specific mold deforms the gland to its *in vivo* shape, but this assumption has not yet been rigorously tested. The use of patient-specific molds, as described by Shah et al, saves time, but at the risk of inaccuracies due to deformation as the prostate is serially sectioned [18]. However, we employed a multi-bladed slicing device, which helped to minimize prostate movement during sectioning.

The low-cost desktop 3D printer (Makerbot Replicator 2) manufactured molds using \$4 worth of material over the course of 6 hours, with minimal human supervision. Furthermore,

3D printed molds for MR-histology correlation

ex vivo prostate geometry was characterized using a low cost 3D scanner, requiring only ten minutes to produce a high-resolution model. Overall the MRI contour matched the *ex vivo* scan closely, with nearly 80% overlap despite a 16% reduction in volume. The prostate contours in the model's coronal and transverse views corresponded to those of the MR surface, but a fairly large discrepancy can be seen in the sagittal view. There, the specimen's anterior base appears truncated relative to the MR surface. This is likely due to tissue manipulation during bladder neck dissection, as well as imprecise segmentation on MR. This discrepancy could have resulted in significant coregistration errors for basal slices, and in future cases 3D scanning will enable compensation for morphological differences such as these.

To date 57 specimens at our institution have been processed using custom molds, and further work is needed to verify our assumptions and to quantitatively evaluate our technique's accuracy. Furthermore, many of these software tasks can be automated, which would improve clinical workflow. To our knowledge there does not yet exist a large-scale study, using sophisticated methods of MR-pathology correlation, for evaluation of cancer extent and refinement of image interpretation. With optimization, our technique could be transformed into a powerful tool for the radiology and pathology community. Improving the predictive capacity of MRI, and understanding its limitations, will be invaluable for future diagnosis and treatment of prostate cancer.

Acknowledgements

We gratefully acknowledge the Jean Perkins Foundation and the Stephen C. Gordon Family Foundation for their financial support. Supported by Award Number R01CA158627 from the National Cancer Institute. The content is solely the responsibility of the authors, and does not necessarily represent the official views of the National Cancer Institute or the National Institutes of Health. JH is supported by a Stand Up To Cancer - Prostate Cancer Foundation Prostate Dream Team Translational Research Grant (SU2C-AACR-DT0812). This research Grant is made possible by the generous support of the Movember Foundation. Stand Up To Cancer is a program of the Entertainment Industry Foundation administered by the American Association for Cancer

Research. JH is also supported by the Department of Defense Prostate Cancer Research Program W81XWH-11-1-0227 and W81XWH-12-1-0206 (PI: Lily Wu), UCLA SPORE in prostate cancer (PI: Robert Reiter), and Prostate Cancer Foundation Honorable A. David Mazzone Special Challenge Award (PI: Robert Reiter).

Disclosure of conflict of interest

None.

Address correspondence to: Alan Priestester, Department of Bioengineering, University of California Los Angeles, CA, USA. E-mail: alanmpriester@gmail.com

References

- [1] Hodge K, McNeal J, Terris M and Stamey T. Random systematic versus directed ultrasound guided transrectal core biopsies of the prostate. *J Urol* 1989; 1: 71-4.
- [2] Hoeks CMA, Barentsz JO, Hambrock T, Yakar D, Somford DM, Heijmink SW, Scheenen TWJ, Vos PC, Huisman H, Van Oort IM, Witjes JA, Heersc-hap A and Fütterer JJ. Prostate Cancer: Multi-parametric MR Imaging for Detection, Localization, and Staging. *Radiology* 2011; 1: 46-66.
- [3] Moore CM, Robertson NL, Arsanious N, Middleton T, Villers A, Klotz L, Taneja SS and Emberton M. Image-guided prostate biopsy using magnetic resonance imaging-derived targets: a systematic review. *Eur Urol* 2013; 1: 125-140.
- [4] Kozlowski P, Chang SD, Jones EC, Berean KW, Chen H and Goldenberg SL. Combined diffusion-weighted and dynamic contrast-enhanced MRI for prostate cancer diagnosis—Correlation with biopsy and histopathology. *J Magn Reson Imaging* 2006; 1: 108-113.
- [5] Sonn GA, Natarajan S, Margolis DJ, MacAiran M, Lieu P, Huang J, Dorey FJ and Marks LS. Targeted biopsy in the detection of prostate cancer using an office based magnetic resonance ultrasound fusion device. *J Urol* 2013; 1: 86-92.
- [6] Selli C, Caramella D, Giusti S, Conti A, Tognetti A, Mogorovich A, De Maria M and Bartolozzi C. Value of image fusion in the staging of prostatic carcinoma. *Radiol Med* 2007; 1: 74-81.
- [7] Husarik DB, Miralbell R, Dubs M, John H, Giger OT, Gelet A, Cserenyák T and Hany TF. Evaluation of [18F]-choline PET/CT for staging and restaging of prostate cancer. *Eur J Nucl Med Mol Imaging* 2008; 2: 253-263.
- [8] Cimitan M, Bortolus R, Morassut S, Canzonieri V, Garbeglio A, Baresic T, Borsatti E, Drigo A and Trovò MG. [18F] fluorocholine PET/CT im-

3D printed molds for MR-histology correlation

- aging for the detection of recurrent prostate cancer at PSA relapse: experience in 100 consecutive patients. *Eur J Nucl Med Mol Imaging* 2006; 12: 1387-1398.
- [9] Haider MA, van der Kwast TH, Tanguay J, Evans AJ, Hashmi AT, Lockwood G and Trachtenberg J. Combined T2-weighted and diffusion-weighted MRI for localization of prostate cancer. *AJR Am J Roentgenol* 2007; 2: 323-328.
- [10] Miao H, Fukatsu H and Ishigaki T. Prostate cancer detection with 3-T MRI: comparison of diffusion-weighted and T2-weighted imaging. *Eur J Radiol* 2007; 2: 297-302.
- [11] Mena E, Turkbey B, Mani H, Adler S, Valera VA, Bernardo M, Shah V, Pohida T, McKinney Y, Kwarteng G, Daar D, Lindenberg ML, Eclarinal P, Wade R, Linehan WM, Merino MJ, Pinto PA. ¹¹C-Acetate PET/CT in localized prostate cancer: a study with MRI and histopathologic correlation. *J Nucl Med* 2012; 4: 538-545.
- [12] Kalavagunta C, Zhou X, Schmechel SC and Metzger GJ. Registration of in vivo prostate MRI and pseudo-whole mount histology using Local Affine Transformations guided by Internal Structures (LATIS). *J Magn Reson Imaging* 2014; [Epub ahead of print].
- [13] Park H, Piert MR, Khan A, Shah R, Hussain H, Siddiqui J, Chenevert TL and Meyer CR. Registration methodology for histological sections and in vivo imaging of human prostate. *Acad Radiol* 2008; 8: 1027-1039.
- [14] Orczyk C, Rusinek H, Rosenkrantz A, Mikheev A, Deng FM, Melamed J and Taneja S. Preliminary experience with a novel method of three-dimensional co-registration of prostate cancer digital histology and *in vivo* multiparametric MRI. *Clin Radiol* 2013; 12: e652-e658.
- [15] Chappelow J, Bloch BN, Rofsky N, Genega E, Lenkinski R, DeWolf W and Madabhushi A. Elastic registration of multimodal prostate MRI and histology via multiattribute combined mutual information. *Med Phys* 2011; 4: 2005-2018.
- [16] Drew B, Jones EC, Reinsberg S, Yung AC, Goldenberg SL and Kozlowski P. Device for sectioning prostatectomy specimens to facilitate comparison between histology and in vivo MRI. *J Magn Reson Imaging* 2010; 4: 992-996.
- [17] Chen LH, Ho H, Lazaro R, Thng CH, Yuen J, Ng WS and Cheng C. Optimum slicing of radical prostatectomy specimens for correlation between histopathology and medical images. *Int J Comput Assist Radiol Surg* 2010; 5: 471-487.
- [18] Shah V, Pohida T, Turkbey B, Mani H, Merino M, Pinto PA, Choyke P and Bernardo M. A method for correlating in vivo prostate magnetic resonance imaging and histopathology using individualized magnetic resonance-based molds. *Rev Sci Instrum* 2009; 10: 104-301.
- [19] Trivedi H, Turkbey B, Rastinehad AR, Benjamin CJ, Bernardo M, Pohida T, Shah V, Merino MJ, Wood BJ, Linehan WM, Venkatesan AM, Choyke PL, Pinto PA. Use of patient-specific MRI-based prostate mold for validation of multiparametric MRI in localization of prostate cancer. *Urology* 2012; 1: 233-239.
- [20] Meyer C, Ma B, Kunju LP, Davenport M and Piert M. Challenges in accurate registration of 3-D medical imaging and histopathology in primary prostate cancer. *Eur J Nucl Med Mol Imaging* 2013; 1: 72-78.
- [21] Natarajan S, Marks LS, Margolis DJ, Huang J, Macairan ML, Lieu P, Fenster A. Clinical application of a 3D ultrasound-guided prostate biopsy system. *Urol Oncol* 2011; 29: 334-342.
- [22] Orczyk C, Mikheev A, Rosenkrantz A, Melamed J, Taneja SS and Rusinek H. Imaging of prostate cancer: A platform for 3D co-registration of in-vivo MRI ex-vivo MRI and pathology. *Proc SPIE* 2012; 8316: 83162M.
- [23] Tan N, Le J, Margolis D, Lu D, King K, Robert R and Raman S. Prostate Cancer Missed by Multi-Parametric MRI: Correlation with Whole-Mount Pathology. *J Urol* 2014; 4: e748-e749.
- [24] Le J, Tan N, Kerkoutian S, Margolis D, Lu D, Kwan L, Raman S and Reiter R. Performance of Multi-Parametric MRI for High-Grade Prostate Cancer: Correlation with Whole-Mount Pathology. *J Urol* 2014; 4: e588.
- [25] Gibson E, Crukley C, Gomez J, Moussa M, Chin J, Bauman G, Fenster A and Ward A. Validation of direct registration of whole-mount prostate digital histopathology to ex vivo MR images. *Prostate Cancer Imaging. Image Analysis and Image-Guided Interventions* 2011; 134-145.
- [26] Hensel JM, Ménard C, Chung PW, Milosevic MF, Kirilova A, Moseley JL, Haider MA and Brock KK. Development of multiorgan finite element-based prostate deformation model enabling registration of endorectal coil magnetic resonance imaging for radiotherapy planning. *Int J Radiat Oncol Biol Phys* 2007; 5: 1522-1528.
- [27] Fan X, Haney CR, Agrawal G, Pelizzari CA, Antic T, Eggener SE, Sethi I, River JN, Zamora M, Karczmar GS, Oto A. High-resolution MRI of excised human prostate specimens acquired with 9.4 T in detection and identification of cancers: Validation of a technique. *J Magn Reson Imaging* 2011; 4: 956-961.
- [28] Ward AD, Crukley C, McKenzie C, Montreuil J, Gibson E, Gomez J, Moussa M, Bauman G and Fenster A. Registration of in vivo prostate magnetic resonance images to digital histopathology images. *Prostate Cancer Imaging Computer-Aided Diagnosis, Prognosis, and Intervention* 2010; 66-76.